Electronic Supplementary Material (ESI) for Physical Chemistry Chemical Physics.
This journal is © the Owner Societies 2016

Supplementary Information to the article ”Hydrogen motions in defective graphene: the role of surface defects”

Chiara Cavallari,[†,‡,‖] Daniele Pontiroli,[‡] Mónica Jiménez-Ruiz,[¶] Mark Johnson,[¶] Matteo Aramini,[‡,⊥] Mattia Gaboardi,[‡] Stewart F. Parker,[§] Mauro Riccó,[‡] and Stéphane Rols[*,†]

†*Institut Laue-Langevin, BP 156, 71 Avenue des Martyrs, 38000 Grenoble, France*

‡*Dipartimento di Fisica e Scienze della Terra, Universitá degli studi di Parma, Via G.Usberti 7/a, 43124 Parma, Italy*

¶*Institut Laue-Langevin, 71 Avenue des Martyrs, 38000 Grenoble, France*

§*ISIS Facility, STFC Rutherford Appleton laboratory, Chilton, Didcot, OX11 0QX, United Kingdom*

‖*Present address: European Synchrotron Radiation Facility, 71 Avenue des Martyrs, 38000 Grenoble, France*

⊥*Present address: Department of Physics, University of Helsinki, Gustaf Hällströmin katu 2b, P.O.B. 64, 00014 Helsinki, Finland*

E-mail: rols@ill.fr

Methods

Sample preparation

The graphene sample under investigation was produced by thermal exfoliation of graphite oxide.[1] Highly pure graphite powder was oxidized following the Brodie method, to obtain graphite oxide (GO). The reduction of GO was achieved by thermal expansion at 1320 K, under dynamical vacuum for 30 min. Thermal exfoliated graphite oxide (TEGO) can be produced in large amounts and the synthesis is in principle scalable to the industrial level. The macro and fine structure of TEGO was previously investigated with TEM, SEM and SAED.[2] Although the material appears more or less disordered, these investigations have clearly shown the presence of both single and few layers structures of sp^2 carbon. A pristine sample was subsequently exposed to thermal annealing at 1073 K under H_2 flux. The so-obtained hydrogenated TEGO (HGr) was the principal subject of our investigations. Hydrogenated nanographite (HBMGr), obtained through by mechanical ball-milling of pure powder graphite and exposed to the same hydrogenation process, was measured as a reference material. Lateral extension of the nanograins in ball-milled graphite (BMGr) has been estimated to be around 6 nm.[3] In order to prevent any possible contamination of the samples with air, all the synthesis steps, hydrogenation procedures and sample handling and storage, were carried out in strictly oxygen free conditions. The amount of H was estimated to be 0.69(2) wt % and 0.21(8) wt % in H-TEGO and H-nanographite, respectively.[4]

Inelastic Neutron scattering

Inelastic neutron scattering (INS) is a highly powerful technique for studying lattice dynamics and atomic and molecular vibrations in materials, especially those containing hydrogen. The observed quantity in a neutron experiment is proportional to the double differential cross section:

$$\frac{\partial^2\sigma}{d\Omega dE} = \left(\frac{\partial^2\sigma}{d\Omega dE}\right)_{coh} + \left(\frac{\partial^2\sigma}{d\Omega dE}\right)_{inc} s \tag{1}$$

which gives the number of neutrons scattered by the sample into a solid angle dΩ around Ω, with a final energy included between E-dE and E+dE. The total intensity and the relative proportion between coherent and incoherent depends on the specific chemical composition of the sample. Hydrogen atoms have the largest and mostly incoherent scattering cross section. Therefore, when performing INS experiment on hydrogenated carbon nanostructures, the spectra will be dominated by the incoherent contributions of ^{1}H atoms. Within the one-phonon and incoherent approximations, the observed quantity in neutron energy loss may be written as:

$$(\frac{\partial^2\sigma}{d\Omega dE}) = \frac{k_f}{k_i}\frac{N}{8\pi}\left[n(\omega,T)+1\right]\frac{Q^2}{\omega}$$
$$\sum_{3N-6}^{j=1}\delta(\omega-\omega_j(\vec{(q)}))\times\sum_{N}^{i=1}\frac{\sigma_i}{M_i}e^{-W_i(\vec{Q})}|\hat{Q}\cdot\hat{e_{ij}}(\vec{Q})|$$

where k_i and k_f are the initial and final neutron wave vectors respectively, Q the modulus of the scattering vector, n(ω,T) the Bose population factor, 2W(Q) the Debye-Waller factor. N is the total number of atoms, σ_i and M$_i$ the total scattering cross-section and the mass of the atom i.[5] In the extent that k_f is much smaller than k_i, the observed intensity in a low-temperature experiment is directly proportional to the generalized density of states. In the case of hydrogenated nanocarbons, due to the predominant ratio $\frac{\sigma_i}{M_i}$ of hydrogen, the measured spectrum is essentially g(E), the partial vibrational density of states of H (HDOS). The IN1-LAGRANGE neutron spectrometer was used to investigate high-frequency vibrations in a wide energy range [50-450meV], where the internal modes of H in carbonaceous matrices are expected. LAGRANGE is located on the hot neutron beamline at the ILL (Grenoble, ILL) and was recently commissioned in replacement of the the previous Beryllium analyser set-up (IN1-BeF). Due to its analyzing set-up, LAGRANGE provides a relatively better energy resolution (approximately 2% in the energy range probed), with respect to the former IN1-BeF. This, together with a very high flux, allows for short acquisition times at various temperatures and makes it particularly suitable to inspect fine features in the spectra and follow the different transformations in great details. Mosaic Cu220 and Cu331 crystal face supplied a monochromatic high energy neutron beam and a cooled polycrystalline Be-filter was used to suppress higher order harmonics. The samples (about 0.3 g) were held at 5 K within a cylindrical aluminum can using a standard Displex cryostat.[6] Data sets were then normalized for monitor counts and corrected for empty cell, background and Debye Waller factor (for measurements collected at 100 K, 200 K and 300 K) using the formula:

$$W(Q) = \frac{Q^2}{4m} \int_0^\infty \frac{g(\omega)}{\omega} coth \frac{\beta\omega}{2} d\omega \tag{2}$$

where Q is the modulus of the scattering vector, ω the frequency in THz, β=1/KT and g(ω) the density of state at the ideal temperature of 0 K. In the calculation, we considered as g(ω) the experimental GDOS collected at 5K, obtained in an energy range as wide as possible by joining data collected on Lagrange and IN4C at the ILL (the latter reported in[4]). Conversion from ω to E follows straighforwardly. Complementary measurements were collected on the chopper spectrometer MAPS at ISIS (Rutherford Appleton Laboratory, Didcot, U.K.).[7]

Computational details

Simulations were performed using the frozen-core all-electron wave (PAW) method,[8] as implemented in the Vienna ab initio DFT code VASP.[9] The electron exchange and correlation are treated within the generalized gradient approximation (GGA) in the Perdew-Burke-Ernzerhof (PBE) form.[10] We used a plane-wave cut-off energy of 500 eV. The relaxation of the atomic positions was performed until all the Hellmann-Feymann forces were converged to 1e-6 eV/Å. Electronic convergence was achieved when the difference between the total energy of the last two successive steps was less then 1e-4 eV. Only the Gamma point in the Brillouin zone was considered for geometry optimization. Optimized structures were used as input for the production of molecular dynamics (MD) trajectories. They were firstly thermal equilibrated at 300 K in the NVT ensemble over 2 ps with a 1.0 fs timestep using the Berendsen thermostat with a velocity scaling each 2 steps. The equilibration run was followed by a production run of 10 ps, performed also in the NVT ensemble; the temperature of 300 K was controlled using the Nose thermostat, with a coupling constant of 96 THz.[11] DOS was computed as time-Fourier transform of the velocity autocorrelation function (VACF) computed from the coordinates of each step of the trajectories, as implemented in the nMOLDYN3 program.[12] The computation of the VACF using an incoherent weight allows extraction of the DOS of the H atoms directly. HDOS were normalized to the number of H atoms for each considered model and convoluted with a Gaussian function, to account for the instrumental resolution. Computational procedure and pseudopotentials were tested by simulating the vibrational density of states of coronene and corannulene. A single molecule was placed in a cubic box with lateral side of 15 Å. Simulated DOS are in very good agreement with both experimental and theoretical results.[13,14] In our experimental conditions, neutron data are directly comparable to simulations.

Models

In the present work, H–graphene configurations were modeled as trigonal graphene supercells with dimensions of 19.7 × 19.7 × 34 Å^3 (8 periodic lengths along a and b directions) with hydrogen atoms chemisorbed atop C atoms at different sites in the graphene lattice. The vacuum thickness along the c-axis was set to 17 Å, in order to avoid possible interactions between neighbour images. A detailed representation of the most significant models is illustrated in Fig. 1. We have considered in-plane configurations of Csp^2-H type, where H saturates in-plane defects, as single atom vacancies (SAV) and more extended inner voids are represented on the left (sketches 1 and 2, respectively), while adatom–like Csp^3-H configurations are depicted on the right: single ad-atom (3), cis-dimers in para (4) and ortho (5) positions (with H adsorbed only on one side of the graphene sheet), trans-dimers in para (6)

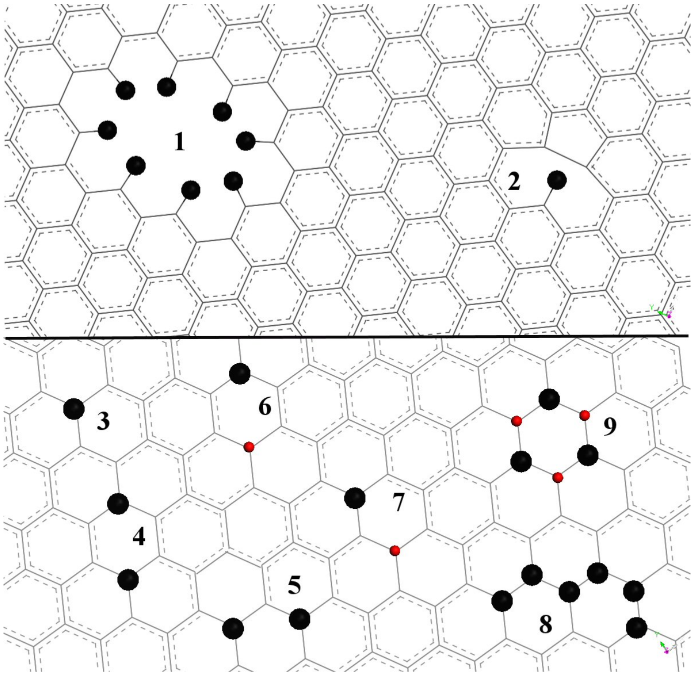

Figure 1: Sketch of some selected C-H configurations that have been considered for a full attribution of the experimental modes through *ab-initio* simulations: in-plane carbon vacancies (top) and chemisorbed H structures onto the plane (bottom). H and C atoms are represented with spheres and thin grey sticks, respectively. H ad-atoms from opposite sides of the sheet are marked with different color and sphere dimension. Only few and the most representative configurations have been depicted as sketches for clarity.

and ortho (7) positions (with H adsorbed on both sides of the graphene sheet in an alternated way), small clusters as cis (8) and trans (9) hexamers.[15] Several other H-graphene configurations were taken into account for simulations like graphane,[16] the fully saturated graphene sheet in both boat and chair conformers and double hydrogenated sites at carbon vacancies and at external edges.[2,17,18] These systems have exhibited poor or not noticeable agreement with the experimental results therefore they have not been illustrated. Graphene fragments characterized by H atoms bonded at the external edges have been modelled as polycyclic aromatic structures of the type $C_{6n^2}H_{6n}$, with n increasing from 2 (this corresponds to coronene molecule) to 4. Calculations of the dynamics have already been published in our previous work.[19]

The simulated HDOS are reported in Fig. 2. Adatom–like configurations share similar vibrational profiles: they all display predominant C-H bending modes in the energy range above 138 meV, peaked around 140/150 meV, while the C-H stretching band is found around 370 meV. By contrast, small monohydrogenated carbon vacancies present C-H bending and stretching modes which match well with the experimental features, having a predominant C-H bending intensity peaked at 108 meV and 118 meV, where the peculiar excess of intensity in HGr is observed. A good match with the C-H stretching frequencies is equally observed. Voids with diameter larger than 12 Å display a HDOS which is very similar to the external edges' response. Nano-sized and even more extended carbon vacancies at the carbon planes, most likely created by the evaporation of chemical groups during the exfoliation process, are expected to fully behave as external edges.

Fig. 3 shows the different contribution to the HDOS in the bending modes range due to C-H bonds placed at strategic position, i.e. showing a different local environment, mainly due to a different number of first neighbours. Isolated H and H at the edges of the cluster give rise to a major peak at 113 meV, being the intensity of the latter one approximately halved as expected from the statistical analysis, while H located in the middle of the cluster gives rise to a vibrational peak sligthly lower in energy. These findings match well with the

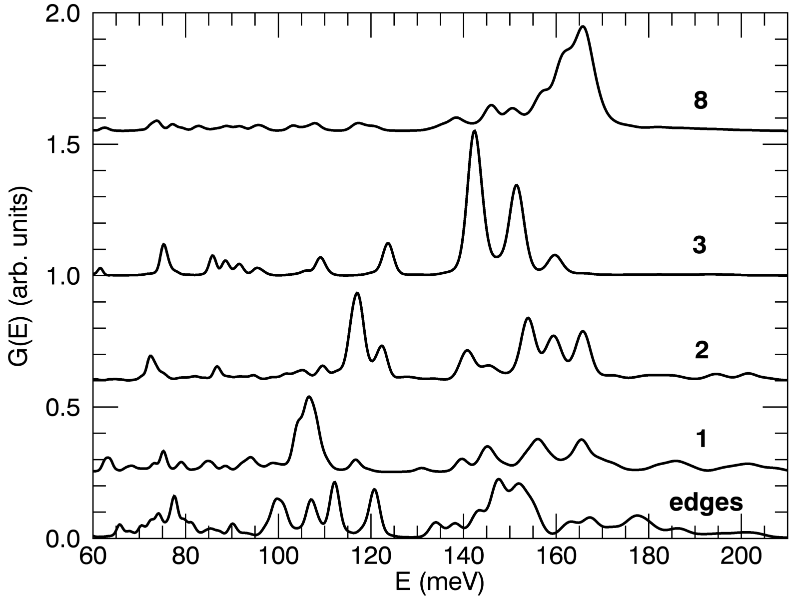

Figure 2: Simulated HDOS in the C-H bending modes range for some selected H-graphene models: external edges,[19] extended carbon vacancy (1), single carbon atom vacancy (2), single H adatom (3), small adatom like cluster (8).

experimental features and the model.

The best agreement between the data collected at 300 K and the simulations is obtained for 30% (edges) + 23% (unsaturated edges - diluted) + 37 % (inner voids) + 10 % (inner voids - diluted), with a total component of around 33 % of C–H in diluted configuration, representing this the mobile C-H component in HGr, as discussed in the main text.

Statistical Model for the H-hopping

The model is constructed as follows: we considered an in-plane void partially populated by H atoms as a 1D array of sites (*i.e.* the carbon atoms) with periodic boundary condition. Let be L the total number of sites in the void and be N the number of hydrogen atoms chemically adsorbed on these sites. The density ρ of H atoms in such a void is therefore $\rho = N/L$.

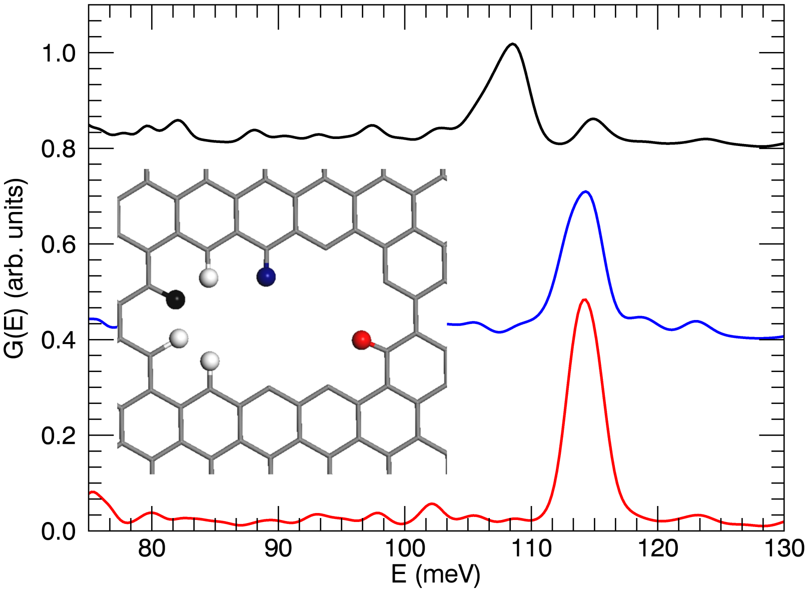

Figure 3: Simulated HDOS and model for an unsatured inner void with H atoms chemisorbed at different positions: in red isolated H, in blue H at the edges of the cluster and in black H inside the cluster.

The energy of the different H arrangements inside the void depends on the H-H interaction ϵ. By restricting our model to first neighbour interactions, we further impose that the total energy of the model E depends only on the number k of H *clusters* present in the void (L, N and ϵ being chosen and kept fixed):

$$E = (N-k)\epsilon \tag{3}$$

Therefore, in the canonical thermodynamics ensemble, the partition function Z can be written as:

$$Z = \sum_{k=1}^{min\{L-N,N\}} \Omega(N,L,k)e^{-\beta(N-k)\epsilon} \tag{4}$$

with $\beta = \frac{1}{k_B T}$ (k_B and T are the Boltzman constant and temperature respectively) and $\Omega(N,L,k)$ being the number of iso-energetic configurations of N H atoms arranged in k clusters positioned on the L-sites chain, and $min\{L-N,N\}$ is the maximum number of cluster possible (depends on the density). We have

$$\Omega(N,L,k) = C^{k-1}_{N-1} C^{k-1}_{L-N-1} \tag{5}$$

with C^{k-1}_{N-1} the number of arrangements of N atoms in k clusters and C^{k-1}_{N-L-1} the number of arrangements of k clusters over L sites (equivalent of arranging $L - N$ voids inside k inter-cluster "boxes"). We have noted $C^m_n = \frac{n!}{(n-m)!m!}$.

Using Eq. 4, one can calculate the Helmoltz free energy $F = -k_B T \ln Z$ and further derive all the thermodynamic functions of the model. In the following, we are interested in calculating the average number of clusters $N_c(T)$ as a function of the temperature of the system. Let us call $P_k(T)$ the probability that the void contains k clusters at a temperature T. We have

$$P_k(T) = \frac{\Omega(N,L,k) e^{-\beta(N-k)\epsilon}}{Z} \tag{6}$$

The average number of clusters N_c is therefore given by:

$$N_c(T) = \sum_{k=1}^{min\{L-N,N\}} k P_k(T) \tag{7}$$

and the average number of H-atoms per cluster is given by $n = \frac{N}{N_c}$. The energy of the system is therefore given by $E = (N - N_c)\epsilon$, and the entropy by $S = \frac{E-F}{T}$

Fig. 4 shows the evolution of N_c with temperature. At low T, N_c=1 which indicates a compact configuration of the H-atoms representing a phase separation between the H-atoms and the H-free carbon sites. As the temperature is increased, the voids can propagate through the H compact phase, rising the number of clusters. This increase depends crucially on ϵ and on the density.

Fig. 5 shows the Helmoltz free energy and its different contributions, i.e. the internal energy of the system and the energy from conformational entropy origin. It clearly shows

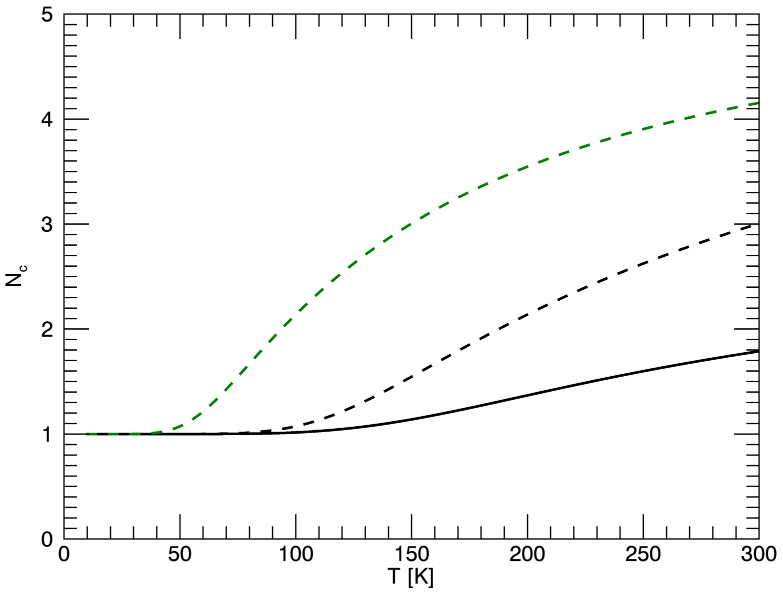

Figure 4: Evolution of the average number of cluster N_c as a function of temperature for different models. Black full line: N=5, L=10 and ϵ=-60 meV, black dashed line: N=10, L=20 and ϵ=-60 meV, green dashed line: N=10, L=20 and ϵ=-30 meV.

that the entropy increase due to the mixing of the H-domains with dangling bonds is not compensated by the increase in energy due to lowering the number of H–H interactions. This is a common feature of low 1D systems with short range interactions, for which the entropy increase by disturbing the local order prevents any phase transition albeit for infinite chains. It was shown for peapods systems that the finite dimension of the chain is responsible for the ordering at rather low temperature,[20,21] a state corresponding to the case N_c=1 for this model. This is an important observation as this behavior is involving the dimension of the H-atoms movements at in-plane voids and H-atoms at the edges of the graphene sheet. Any compaction of the sheets are likely to increase the dimension of the system and therefore play an important role on the localization of the H-atoms.

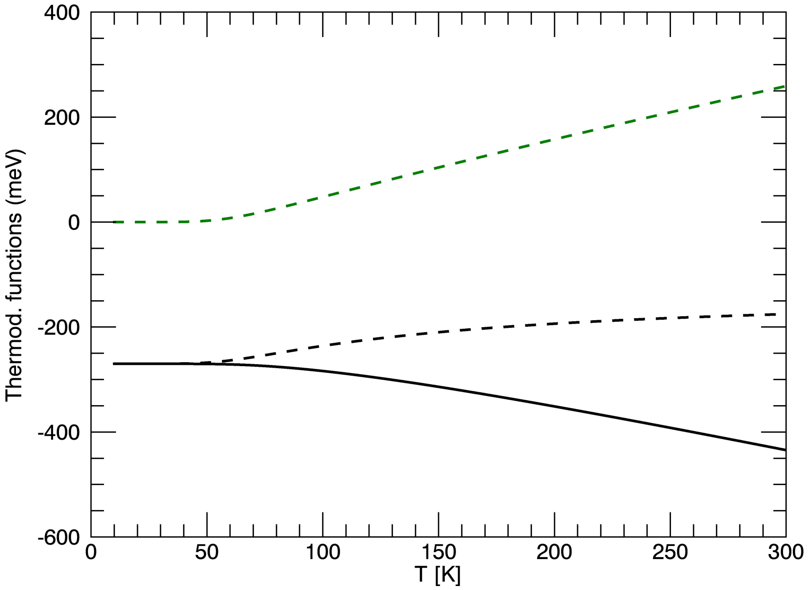

Figure 5: The free energy F (full black line), the energy E (dashed black line) and the entropy term of the energy TS (dashed green line) as a function of temperature for the model N=10, L=20 and ϵ=-30 meV.

References

1. Park, S.; Ruoff, R. S. Chemical methods for the production of graphenes. *Nat Nano* **2009**, *4*, 217–224.

2. Riccò, M.; Pontiroli, D.; Mazzani, M.; Choucair, M.; Stride, J. A.; Yazyev, O. V. Muons probe strong hydrogen interactions with defective graphene. *Nano letters* **2011**, *11*, 4919–4922.

3. Makarova, T.; Riccò, M.; Pontiroli, D.; Mazzani, M.; Belli, M.; Goffredi, A. Ageing effects in nanographite monitored by Raman spectroscopy. *physica status solidi (b)* **2008**, *245*, 2082–2085.

4. Pontiroli, D.; Aramini, M.; Gaboardi, M.; Mazzani, M.; Sanna, S.; Caracciolo, F.; Carretta, P.; Cavallari, C.; Rols, S.; Tatti, R. *et al.* Tracking the Hydrogen Motion in Defective Graphene. *The Journal of Physical Chemistry C* **2014**, *118*, 7110–7116.

5. Lovesey, S. In *Theory of Neutron Scattering from Condensed Matter*, 3rd ed.; Publications, O. S., Ed.; The International Series of Monographs on Physics, 1987.

6. Jimenez-Ruiz, M.; Ivanov, A.; Fuard, S. LAGRANGE - the new neutron vibrational spectrometer at the ILL. *Journal of Physics: Conference Series* **2014**, *549*, 012004.

7. Parker, S. F.; Ramirez-Cuesta, A. J.; Albers, P. W.; Lennon, D. The use of direct geometry spectrometers in molecular spectroscopy. *Journal of Physics: Conference Series* **2014**, *554*, 012004.

8. Blöchl, P. E. Projector augmented-wave method. *Physical Review B* **1994**, *50*, 17953.

9. Kresse, G.; Furthmüller, J. Efficient iterative schemes for ab initio total-energy calculations using a plane-wave basis set. *Physical Review B* **1996**, *54*, 11169.

10. Perdew, J. P.; Burke, K.; Ernzerhof, M. Generalized Gradient Approximation Made Simple. *Phys. Rev. Lett.* **1996**, *77*, 3865–3868.

11. Nosé, S. A unified formulation of the constant temperature molecular dynamics methods. *The Journal of chemical physics* **1984**, *81*, 511–519.

12. Calandrini, V.,; Pellegrini, E.,; Calligari, P.,; Hinsen, K.,; Kneller, G.R., nMoldyn - Interfacing spectroscopic experiments, molecular dynamics simulations and models for time correlation functions. *JDN* **2011**, *12*, 201–232.

13. Mitchell, P. C. H.; Ramirez-Cuesta, A. J.; Parker, S. F.; Tomkinson, J. Inelastic neutron scattering in spectroscopic studies of hydrogen on carbon-supported catalysts-experimental spectra and computed spectra of model systems. *Journal of molecular structure* **2003**, *651*, 781–785.

14. Le Parc, R.; Hermet, P.; Rols, S.; Maurin, D.; Alvarez, L.; Ivanov, A.; Quimby, J. M.; Hanley, G., Caitlin; Scott, L. T.; Bantignies, J.-L. New Insights on Vibrational Dynamics of Corannulene. *The Journal of Physical Chemistry C* **2012**, *116*, 25089–25096.

15. Šljivančanin, i. c. v.; Andersen, M.; Hornekær, L.; Hammer, B. Structure and stability of small H clusters on graphene. *Phys. Rev. B* **2011**, *83*, 205426.

16. Sofo, J. O.; Chaudhari, A. S.; Barber, G. D. Graphane: A two-dimensional hydrocarbon. *Phys. Rev. B* **2007**, *75*, 153401.

17. Casartelli, M.; Casolo, S.; Tantardini, G. F.; Martinazzo, R. Structure and stability of hydrogenated carbon atom vacancies in graphene. *Carbon* **2014**, *77*, 165 – 174.

18. Papanek, P.; Kamitakahara, W. A.; Zhou, P.; Fischer, J. E. Neutron scattering studies of disordered carbon anode materials. *Journal of Physics: Condensed Matter* **2001**, *13*, 8287.

19. Cavallari, C.; Pontiroli, D.; Jiménez-Ruiz, M.; Ivanov, A.; Mazzani, M.; Gaboardi, M.; Aramini, M.; Brunelli, M.; Riccò, M.; Rols, S. Hydrogen on graphene investigated by inelastic neutron scattering. *Journal of Physics: Conference Series* **2014**, *554*, 012009.

20. Bousige, C.; Rols, S.; Paineau, E.; Rouzière, S.; Mocuta, C.; Verberck, B.; Wright, J. P.; Kataura, H.; Launois, P. Progressive melting in confined one-dimensional C_{60} chains. *Phys. Rev. B* **2012**, *86*, 045446.

21. Hodak, M.; Girifalco, L. A. Quasi-one-dimensional system of molecules inside carbon nanotubes: Exact solution for the lattice gas model and its application to fullerene-filled nanotubes. *Phys. Rev. B* **2001**, *64*, 035407.